Available online at www.sciencedirect.com
SCIENCE DIRECT®
Journal of Computational Physics 208 (2005) 651–674
JOURNAL OF COMPUTATIONAL PHYSICS
www.elsevier.com/locate/jcp

Wave field simulation for heterogeneous porous media with singular memory drag force

Jian-Fei Lu [a,b,*], Andrzej Hanyga [b]

[a] *Mathematics and Physics Institute of JiangSu University, ZhenJiang, JiangSu 212013, PR China*
[b] *Institute of Earth Science, University of Bergen, Allegaten 41, N5007 Bergen, Norway*

Received 8 December 2004; received in revised form 28 February 2005; accepted 2 March 2005
Available online 5 May 2005

Abstract

The objective of this paper is to use Biot's theory and the Johnson–Koplik–Dashen dynamic permeability model in wave field simulation of a heterogeneous porous medium. The Johnson–Koplik–Dashen dynamic permeability model was originally formulated in the frequency domain. In this paper, the time domain drag force expression of the model is expressed in terms of the shifted fractional derivative of the relative fluid velocity. In contrast to the exponential-type viscous relaxation models, the convolution operator in the Johnson–Koplik–Dashen dynamic permeability model cannot be replaced by memory variables satisfying first-order relaxation differential equations. A new method for calculating the shifted fractional derivative without storing and integrating the entire velocity histories is developed. Using the new method to calculate the fractional derivative, the governing equations for the two-dimensional porous medium are reduced to a system of first-order differential equations for velocities, stresses, pore pressure and the quadrature variables associated with the drag forces. Spatial derivatives involved in the first-order differential equations system are calculated by Fourier pseudospectral method, while the time derivative of the system is discretized by a predictor–corrector method. For the demonstration of our method, some numerical results are presented.

Keywords: Porous medium; Dynamic permeability; Fractional derivative; Singular memory; Drag force; Fourier pseudospectral method

1. Introduction

The mechanics of porous media has important applications in geophysics, in particular, in seismology, geotechnical engineering and petroleum engineering. For example, successful oil recovery depends

* Corresponding author. Tel.: +47 55583424; fax: +47 5118780047.
E-mail addresses: ljfdoctor@yahoo.com (J.-F. Lu), andrzej.hanyga@geo.uib.no (A. Hanyga).

0021-9991/$ - see front matter © 2005 Elsevier Inc. All rights reserved.
doi:10.1016/j.jcp.2005.03.008

on the seismic monitoring of the fluid flow in a porous reservoir. It is believed that pore fluids play an important role in the generation of earthquakes. Liquefaction of saturated sand due to dynamic loads has been an important topic in earthquake engineering for a long time. The first theory of wave propagation in a fluid-saturated porous medium was put forward by Biot [1,2]. Biot's theory was also extended to include anisotropy and viscoelastic properties of the matrix [3]. The most important achievement of Biot's theory was the prediction of the second kind P-wave in one-fluid-saturated porous medium [4]. After the establishment of Biot's theory, many investigators have used it to study the wave propagation in a porous medium. For example, the propagation of Rayleigh waves in saturated poroelastic half-space was studied by Jones [5] and Deresiewicz [6]. Deresiewicz and Skalak [7] studied the question of uniqueness of solutions for Biot's equations and the corresponding boundary conditions for the solutions. Also, dynamic Green's function for a two-dimensional half space was developed by Senjuntichai and Rajapakse [8]. Norris [9] derived the Green's function for a point force applied in an unbounded poroelastic medium in frequency domain. Based on the Green's function for four independent variables (three for the skeleton displacements and one for pore pressure), the frequency domain boundary element method for homogeneous porous medium was developed by Zimmerman and Stern [10]. More recently, the asymptotic ray theory for porous medium was developed by Hanyga and Seredynska [11] and the time domain asymptotic Green's functions have been obtained in explicit form in [12].

However, one may find that up to now the research concerning saturated porous medium has been mainly limited to the homogeneous case, while the research on heterogeneous porous media is in a preliminary stage. Recently, with the development of algorithm for numerical schemes for partial differential equation and computer technology, the inhomogeneous wave field calculation for porous medium begins to attract the attention of researchers. For example, Ozdenvar and McMechan [13] developed a staggered-grid algorithm for computation of wave propagation in an inhomogeneous porous medium in terms of displacement formulation. However, the drag force between the fluid and the solid skeleton is assumed to be a linear function of the relative velocity, which is valid only in the low-frequency approximation. The low-frequency approximation only applies to signal frequency ranges below the characteristic frequency of the medium [1,2]. Carcione [14] developed an algorithm for a heterogeneous linear anisotropic porous medium. In Carcione's work both the low-frequency range and the high-frequency range are considered. For the high-frequency range, the drag force relaxation is represented by a exponential-type kernel. Therefore, the convolutions involved in the drag forces are eliminated by introduction of corresponding internal variables [15]. The exponential-type relaxation function and corresponding derivative are bounded at small times. However, there is ample experimental and theoretical evidence to the effect that the viscoelastic relaxation function or its derivatives are unbounded at $t \to 0$. In particular, it has been justified by the dynamic permeability theory [16] of a saturated porous medium that the drag force model should be consistent with the presence of boundary layer thickness $\delta\omega^{-1/2}$ for the high-frequency range where δ is a constant. This implies that the memory effect for the drag force should be expressed in terms of a time convolution with a singularity $t^{-1/2}$ for $t \to 0$. For example, the Biot model [2], the Johnson–Koplik–Dashen (JKD) model [16], the Pride–Morgan–Gangi (PMG) model [17] and several poroelastic models [18–20] all exhibit such a singularity. In contrast to Biot's model [2] which is based on the artificial assumption of circular pores of constant cross- section, the JKD and PMG models, due to the algebraic dependence of drag force/dynamic permeability on the frequency, can be relatively easily expressed in terms of an explicit time domain operator and implemented in a time domain numerical scheme. As shown in a review paper [21], current poroelastic models based on double porosity, patchy saturation and squirt flow consistently lead to the same frequency dependence of the effective dynamic permeability. In saturated porous media, memory effects are normally expected to be relevant for signals involving frequencies of order of the transition frequencies. In the case of Biot's model of a microhomogeneous porous medium, the transition frequency lies at about 10^5Hz. However,

increasing theoretical [22–24] and experimental [25] evidences indicate that for rocks, which are heterogeneous on a scale intermediate between the pore dimensions and the wavelength, the associated attenuation reduces the threshold of memory effects to frequencies of order 10–100 Hz. Consequently, the memory effects associated with drag force are relevant not only to ultrasound but also to seismic wave propagation.

Explicit drag forces accounting for the interaction between the pore fluid and the pore walls have been determined for some specific pore geometries, for example, aligned pores with circular, triangular or rectangular cross-section [2]. Pride et al. [17] derived the drag force model for more general pore geometry. In 1987, Johnson, Koplik and Dashen [16] put forward a general model of dynamic permeability. Johnson et al. pointed out that dynamic permeability $\tilde{k}(\omega)$ should satisfy the following conditions: (a) the dynamic permeability function should be analytical function for the ω in the upper half-plane; (b) $\tilde{k}(\omega)$ should have the following symmetry $\tilde{k}(-\omega) = \tilde{k}^*(\omega)$, where the asterisk denotes complex-conjugation; (c) the limit of low frequency is equal to the value for static case; (d) in the limit of high frequency the thickness of boundary layer must be smaller than all characteristic pore size. Johnson, Koplik and Dashen [16] also put forward a general frequency-dependent model of dynamic permeability, which we henceforth call the JKD model, to account for the interaction between the solid skeleton and the fluid. It is worth noting that except for the difference in the specific expressions for the dynamic permeability, the JKD model is in agreement with Biot's theory, since separate inertia interaction and viscous interaction can also be obtained in the context of the JKD model. In the present paper, the term drag force refers to the viscous interaction force between the solid skeleton and the fluid. Due to generality of the JKD model, it has been used in many papers on acoustics of porous media [26,27] and on electro-seismology [28,29]. Moreover, Charlaix et al. [30] have experimentally measured the dynamic permeability for samples of fused-glass beads and crushed glass. They observed that generally the JKD model match experimental data very well. Zhou and Sheng [31] applied the finite-element method to model the dynamic permeability for a variety of specific pore models that have variable-width flow channels and they also found generally the JKD model could give satisfactory results.

The objective of this paper is to combine Biot's theory with the JKD dynamic permeability and use them in wave field simulation of a heterogeneous saturated porous medium. The JKD model of porous medium was originally formulated in the frequency domain [16]. However, for wave field simulation of a heterogeneous porous medium, a time domain expression of the JKD model is required. In this paper, using the shifted fractional derivative operator, the explicit time domain drag force in the JKD model is derived for the first time. In the time domain the JKD dynamic permeability is expressed by the shifted fractional derivative of relative fluid velocity. The shifted fractional derivative of relative velocity is equivalent to a time convolution of a kernel having singularity at initial time with the relative velocity. In contrast to the exponential drag force models [14], the convolution operator in the JKD model cannot be eliminated by introducing a finite number of memory variables satisfying first-order differential relaxation equations. Therefore, in order to avoid storage and integration of the entire velocity history required for evaluation of the fractional derivative, a new method, which is based on the Yuan and Agrawal's method [32] and the asymptotic analysis of the infinite integral equivalent to the fractional derivative, for calculating the fractional derivative is developed. Using the new method to evaluate the fractional derivative, a system of first-order differential equations for velocities, stresses, pore pressure and the quadrature variables associated with the shifted fractional derivatives is derived from the governing equations for the two-dimensional porous medium. Spatial derivatives involved in the first-order differential equations system are calculated by Fourier pseudospectral method, while the time derivative of the system is discretized by a predictor–corrector method. For the demonstration of our method, some numerical results are given in the paper.

2. Incorporation of the JKD model with Biot's theory in time domain

2.1. Definition of shifted fractional derivative operators

The drag force in the JKD model can be expressed in terms of the shifted fractional derivative [30], which we now briefly introduce here. The shifted fractional derivative operator $(D+\lambda)^{\alpha}$ is defined by the following formula [33]:

$$(D+\lambda)^{\alpha} f(t) = \mathrm{e}^{-\lambda t} D^{\alpha}[\mathrm{e}^{\lambda t} f(t)], \tag{1}$$

where $\lambda \geqslant 0$ and $0 < \alpha < 1$, D^{α} represents the Caputo fractional derivative [34]. For the convenience of the derivation in the following section, we need the Laplace transform of the shifted fractional derivative. The Laplace transformation is defined as follows:

$$L[f(t)](s) = \int_0^{\infty} f(t)\mathrm{e}^{-st}\,\mathrm{d}t. \tag{2}$$

The Laplace transform of the shifted fractional derivative can be calculated using the Laplace transformation of the Caputo derivative [34]

$$\begin{aligned} L[(D+\lambda)^{\alpha} f(t)](s) &= L[\mathrm{e}^{-\lambda t} D^{\alpha}(\mathrm{e}^{\lambda t} f(t))](s) = L[D^{\alpha}(\mathrm{e}^{\lambda t} f(t))](s+\lambda) \\ &= (s+\lambda)^{\alpha} L[\mathrm{e}^{\lambda t} f(t)](s+\lambda) - f(0^{+})(s+\lambda)^{\alpha-1} = (s+\lambda)^{\alpha}\tilde{f}(s) - f(0^{+})(s+\lambda)^{\alpha-1}. \end{aligned} \tag{3}$$

Applying the inverse Laplace transformation to the above equation, one has

$$L^{-1}[(s+\lambda)^{\alpha}\tilde{f}(s)] = (D+\lambda)^{\alpha} f(t) + f(0^{+})\mathrm{e}^{-\lambda t}\frac{t^{-\alpha}}{\Gamma(1-\alpha)}, \tag{4}$$

where L^{-1} denotes the inverse Laplace transformation and Γ denotes the Gamma function.

2.2. The JKD model

As is well known, the JKD model was originally formulated in the frequency domain. In this section, by using the shifted fractional derivative operator, the time domain drag force in the JKD model is derived for the first time.

If the acceleration of the solid skeleton is zero, the Darcy law for porous fluid flow induced by the gradient of pore pressure ∇p has the following form [35]:

$$\partial_t \mathbf{w} := \phi(\partial_t \mathbf{U} - \partial_t \mathbf{u}) = -\frac{k_0}{\eta}\nabla p, \tag{5}$$

where $\mathbf{U}$ is the displacement for porous fluid, $\mathbf{u}$ is displacement the solid skeleton, $\mathbf{w}$ is the relative displacement between the solid and fluid, ϕ is the porosity, k_0 is the dc permeability and η is the viscosity of the fluid. The frequency domain Darcy law with inertial effects of the fluid included has the following form:

$$\mathrm{i}\omega\tilde{\mathbf{w}} = \frac{\tilde{k}(\omega)}{\eta}(-\nabla\tilde{p} + \rho_{\mathrm{f}}\omega^2\tilde{\mathbf{u}}), \tag{6}$$

where $\tilde{k}(\omega)$ is the dynamic permeability, ω is angular frequency and ρ_{f} is the density of the pore fluid and the common time factor $\mathrm{e}^{\mathrm{i}\omega t}$ is omitted here. In frequency domain, according to the JKD model, the dynamic permeability has the following form [16]

$$\tilde{k}(\omega) = k_0 \left[\left(1 + \mathrm{i} \frac{4a_\infty^2 k_0^2 \rho_\mathrm{f} \omega}{\Lambda^2 \phi^2 \eta} \right)^{1/2} + \mathrm{i} \frac{\omega a_\infty \rho_\mathrm{f} k_0}{\phi \eta} \right]^{-1}, \tag{7}$$

where a_∞ is tortuosity and Λ has the dimension of length. Substitution of Eq. (7) into Eq. (6) yields

$$\mathrm{i}\omega\tilde{\mathbf{w}} \left[\left(1 + \mathrm{i} \frac{4a_\infty^2 k_0^2 \rho_\mathrm{f} \omega}{\Lambda^2 \phi^2 \eta} \right)^{1/2} + \mathrm{i} \frac{\omega a_\infty \rho_\mathrm{f} k_0}{\phi \eta} \right] = \frac{k_0}{\eta} (-\nabla p + \rho_\mathrm{f} \omega^2 \tilde{\mathbf{u}}). \tag{8}$$

Introducing the transition frequency ω_T which separates the viscous-force-dominated flow from the inertial-force-dominated flow and the geometrical factor K [16]

$$\omega_\mathrm{T} = \frac{\eta \phi}{\rho_\mathrm{f} a_\infty k_0}, \quad K = \frac{4 a_\infty k_0}{\Lambda^2 \phi}. \tag{9a, b}$$

Eq. (8) is recast in the following form:

$$-\nabla \tilde{p} = -\rho_\mathrm{f} \omega^2 \tilde{\mathbf{u}} - m\omega^2 \tilde{\mathbf{w}} + \frac{\eta}{k_0} a_\mathrm{s}^{-\frac{1}{2}} (\mathrm{i}\omega + a_\mathrm{s})^{1/2} \mathrm{i}\omega \tilde{\mathbf{w}}, \tag{10}$$

where $m = a_\infty \rho_\mathrm{f}/\phi$, $a_\mathrm{s} = \omega_\mathrm{T}/K$.

If substituting $\mathrm{i}\omega$ with s in the above equation and performing the inverse Laplace transformation on the resulting equation and using Eq. (4), the following equation is obtained:

$$-\nabla p = \rho_\mathrm{f} \ddot{\mathbf{u}} + m\ddot{\mathbf{w}} + \frac{\eta}{k_0} a_\mathrm{s}^{-\frac{1}{2}} (D + a_\mathrm{s})^{1/2} \dot{\mathbf{w}}, \tag{11}$$

where a superimposed dot on a variable denotes time derivative. Note that in deriving Eq. (11), the zero initial condition for $\mathbf{u}, \dot{\mathbf{u}}, \mathbf{w}, \dot{\mathbf{w}}$ is assumed. It follows from Eq. (11) that the interaction between the pore fluid and the solid skeleton consists of an inertia interaction part (the second term of the right-hand side of (11)) and a viscous interaction part (the third term of the right-hand side of (11)). As mentioned above, the viscous term is defined as drag force in this paper. Note that the drag force here is represented by a shifted fractional derivative of the relative velocity $\dot{\mathbf{w}}$ of order 1/2. In view of the non-locality of the fractional derivative, the drag force at a fixed time depends on the entire history of velocity $\dot{\mathbf{w}}$.

2.3. Combination of JKD model with Biot's theory in time domain

Consider an unbounded heterogeneous porous medium in a Cartesian co-ordinate system xyz. The constitutive equations of Biot's theory of a saturated porous medium have the following form [3]:

$$\sigma_{ij} = 2\mu\varepsilon_{ij} + \lambda\delta_{ij} e - \alpha\delta_{ij} p, \tag{12a}$$

$$p = -\alpha M e + M\vartheta, \tag{12b}$$

where

$$\varepsilon_{ij} = \frac{1}{2}(u_{i,j} + u_{j,i}), \quad e = u_{i,i}, \quad \vartheta = -w_{i,i}. \tag{13a–c}$$

In the above equations, σ_{ij} denotes the stress of the bulk material; p is the excess pore pressure and δ_{ij} is the Kronecker delta; ε_{ij}, e are the strain tensor and the dilatation of the solid skeleton; ϑ is the volume of fluid injection into unit volume of bulk material; λ, μ are the Lame constants of the solid skeleton; α, M are the Biot parameters [36] accounting for the compressibility of the saturated two-phase porous medium.

Combining Eqs. (12) and (13) with Eq. (11), the following equations of the motion for the bulk material and the pore fluid are obtained:

$$\sigma_{ij,j} + F_i^{\mathrm{b}} = \rho\ddot{u}_i + \rho_{\mathrm{f}}\ddot{w}_i, \tag{14a}$$

$$-p_{,i} + F_i^{\mathrm{f}} = \rho_{\mathrm{f}}\ddot{u}_i + m\ddot{w}_i + \frac{k_0}{\eta}a_{\mathrm{s}}^{-\frac{1}{2}}(D + a_{\mathrm{s}})^{1/2}\dot{w}_i, \tag{14b}$$

where ρ denote the bulk density of the porous material and $\rho = (1-\phi)\rho_{\mathrm{s}} + \phi\rho_{\mathrm{f}}$, ρ_{s} is the density of the solid skeleton; $F_i^{\mathrm{b}}, F_i^{\mathrm{f}}$ are the body force for a unit volume of the bulk material and the pore fluid.

2.4. Numerical comparison between the low-frequency approximation and the JKD model

In this section, we shall use a point force solution to demonstrate the difference between the low-frequency approximation and the JKD model. Suppose a vertical point force is applied at an unbounded two-dimensional porous medium. The low-frequency approximation with drag force denoted by the product of the velocity and a constant and the JKD model are used in the calculation. The parameters for the porous medium are as follows: $\rho_{\mathrm{f}} = 1.0\times10^3\ \mathrm{kg/m^3}$, $\rho_{\mathrm{s}} = 2.0\times10^3\ \mathrm{kg/m^3}$, $\phi = 0.3$, $\lambda = 1.0\times10^9\ \mathrm{Pa}$, $\mu = 2.0\times10^9\ \mathrm{Pa}$, $\alpha = 0.9$, $M = 1.0\times10^{10}\ \mathrm{Pa}$, $\eta = 1.0\times10^{-3}\ \mathrm{Pa\,s}$, $k_0 = 4.0\times10^{-12}\ \mathrm{m^2}$, $a_\infty = 3.0$, $K = 0.5$. The point force is of the shape of a Ricker wavelet [37] and is applied at the origin o. The value of vertical force is given by

$$S(t) = FR(t), \tag{15}$$

where F is of the dimension N/L and $R(t)$ is the Ricker wavelet [37] given by

$$R(t) = \left[\frac{\omega_{\mathrm{c}}^2(t-t_{\mathrm{s}})^2}{2} - 1\right]\mathrm{e}^{-\frac{\omega_{\mathrm{c}}^2(t-t_{\mathrm{s}})^2}{4}}. \tag{16}$$

The central frequency f_{c} and the time shift t_{s} of the vertical force are $f_{\mathrm{c}} = 2\times10^5\ \mathrm{Hz}$, and $t_{\mathrm{s}} = 10^{-5}\ \mathrm{s}$, where $f_{\mathrm{c}} = \omega_{\mathrm{c}}/(2\pi)$. The receiver is located at $(x,z) = (0.1\,\mathrm{m}, 0.2\,\mathrm{m})$ where x, z are horizontal and vertical coordinates, respectively. In terms of reference length, reference shear modulus and reference density $a_{\mathrm{r}}, \mu_{\mathrm{r}}, \rho_{\mathrm{r}}$, reference time is $t_{\mathrm{r}} = a_{\mathrm{r}}\sqrt{\rho_{\mathrm{r}}/\mu_{\mathrm{r}}}$.

We shall use the potential method as well as the FFT method to calculate the time domain solution of the point force. In the frequency domain, all the variables of the two-dimension porous medium can be represented by three potentials satisfying the following Helmholtz equations [10,38]:

$$\nabla^2\varphi_{\mathrm{f}} + k_{\mathrm{f}}^2\varphi_{\mathrm{f}} = 0, \tag{17a}$$

$$\nabla^2\varphi_{\mathrm{s}} + k_{\mathrm{s}}^2\varphi_{\mathrm{s}} = 0, \tag{17b}$$

$$\nabla^2\psi + k_t^2\psi = 0, \tag{17c}$$

where $\varphi_{\mathrm{f}}, \varphi_{\mathrm{s}}, \psi$ are the potentials for the fast P wave, slow P wave and S wave, respectively, and $k_{\mathrm{f}}, k_{\mathrm{s}}, k_{\mathrm{t}}$ are the corresponding complex wave numbers, and $k_{\mathrm{f}}^2 = (\beta_5 A_{\mathrm{f}} - \beta_4)/A_{\mathrm{f}}$, $k_{\mathrm{s}}^2 = (\beta_5 A_{\mathrm{s}} - \beta_4)/A_{\mathrm{s}}$, $k_t^2 = \beta_3/\mu$, $\beta_2 = \alpha - \rho_{\mathrm{f}}\omega^2/\beta_1$, $\beta_3 = \rho\omega^2 - \rho_{\mathrm{f}}^2\omega^4/\beta_1$, $\beta_4 = \rho_{\mathrm{f}}\omega^2 - \alpha\beta_1$, $\beta_5 = \beta_1/M$. For the JKD model assumed here $\beta_1 = m\omega^2 - \mathrm{i}\omega\eta(1 + \mathrm{i}\omega K/\omega_{\mathrm{T}})^{1/2}/k_0$, A_{f}, A_{s} are the solutions of the following equation:

$$A_{\mathrm{f,s}}^2 + \frac{\beta_3 - \beta_2\beta_4 - (\lambda+2\mu)\beta_5}{\beta_2\beta_5}A_{\mathrm{f,s}} + \frac{(\lambda+2\mu)\beta_4}{\beta_2\beta_5} = 0. \tag{18}$$

The solid and fluid displacements and the pore pressure are given by the following expressions:

$$u_x = \frac{\partial\varphi_{\mathrm{f}}}{\partial x} + \frac{\partial\varphi_{\mathrm{s}}}{\partial x} + \frac{\partial\psi}{\partial z}, \tag{19a}$$

$$u_z = \frac{\partial \varphi_f}{\partial z} + \frac{\partial \varphi_s}{\partial z} - \frac{\partial \psi}{\partial x}, \tag{19b}$$

$$w_x = \eta_1 \frac{\partial \varphi_f}{\partial x} + \eta_2 \frac{\partial \varphi_s}{\partial x} + \alpha_1 \frac{\partial \psi}{\partial z}, \tag{19c}$$

$$w_z = \eta_1 \frac{\partial \varphi_f}{\partial z} + \eta_2 \frac{\partial \varphi_s}{\partial z} - \alpha_1 \frac{\partial \psi}{\partial x}, \tag{19d}$$

$$p = -A_f k_f^2 \varphi_f - A_s k_s^2 \varphi_s, \tag{19e}$$

where $\eta_1 = \alpha_1 - A_f k_f^2/\beta_1$, $\eta_2 = \alpha_1 - A_s k_s^2/\beta_1$, $\alpha_1 = -\rho_f \omega^2/\beta_1$. Note that the stresses of the porous medium can be evaluated by the constitutive relations (12a).

In order to solve the full plane porous medium problem of the point force, we divide the full plane into two domains: domain D_1 above the level of attachment of the point force and domain D_2 below that level. The following continuity conditions are satisfied at the horizontal plane passing through the point force:

$$\begin{aligned} &u_{x_1}(x,0^-,\omega) = u_{x_2}(x,0^+,\omega), \quad u_{z_1}(x,0^-,\omega) = u_{z_2}(x,0^+,\omega),\\ &w_{z_1}(x,0^-,\omega) = w_{z_2}(x,0^+,\omega), \quad \sigma_{zx_1}(x,0^-,\omega) = \sigma_{zx_2}(x,0^+,\omega),\\ &p_1(x,0^-,\omega) = p_2(x,0^+,\omega), \quad \sigma_{zz_2}(x,0^+,\omega) - \sigma_{zz_1}(x,0^-,\omega) = -\delta(x) F \tilde{R}(\omega), \end{aligned} \tag{20a–f}$$

where $\tilde{R}(\omega)$ is the Fourier transform of the Ricker wavelet. Applying Fourier transformation to variable x in Eq. (17), the general solutions involving six arbitrary constants for the potentials $\varphi_{f_1}, \varphi_{s_1}, \psi_1(D_1)$ and $\varphi_{f_2}, \varphi_{s_2}, \psi_2(D_2)$ are obtained. Applying the Fourier transformation to variable x in Eq. (19) and substituting the expressions of the potentials, the expressions for displacements, stresses and pore pressure are obtained. Applying the Fourier transformation to variable x in Eq. (20) and substituting the expressions of displacements, stresses and pore pressure, the six arbitrary constants involved in the potentials can be determined. After determining the potentials, the frequency domain solutions can be evaluated by numerical inversion of the Fourier transformation, while the time domain solution can be obtained by using the FFT method.

The non-dimensional velocity v_z, stress σ_{zz} and pore pressure p are presented in Figs. 1(a)–(c). These results show that the low-frequency approximation gives smaller attenuation than the JKD model. It is well known [39], Biot's theory tends to predict significantly lower attenuation compared with experimental results for rocks. However, this situation can be partly improved if an appropriate dynamic permeability model is used. Therefore, the singular memory effect here accounts for the additional attenuation in the context of Biot's theory.

2.5. Velocity–stress formulation for two-dimensional porous elastic medium

In this section, the velocity–stress formulation for the two-dimensional porous media will be constructed. As is well known, the velocity–stress formulation can eliminate the differentiation of the material parameters along with the associated numerical artifacts and makes the algorithm more stable [40].

We introduce the following velocities for the solid skeleton and the pore fluid

$$v_x(t) = \dot{u}_x(t), \quad v_z(t) = \dot{u}_z(t), \quad q_x(t) = \dot{w}_x(t), \quad q_z(t) = \dot{w}_z(t). \tag{21a–d}$$

Then, in terms of Eqs. (14) and (21), one has

$$\dot{v}_x(t) = \frac{m\gamma_s}{\rho_f}(\sigma_{xx,x} + \sigma_{xz,z}) + \gamma_s p_{,x} + \frac{\eta}{k_0}\gamma_s a_s^{-\frac{1}{2}}(D + a_s)^{1/2} q_x + \gamma_s\left(\frac{m}{\rho_f}F_x^b - F_x^f\right), \tag{22a}$$

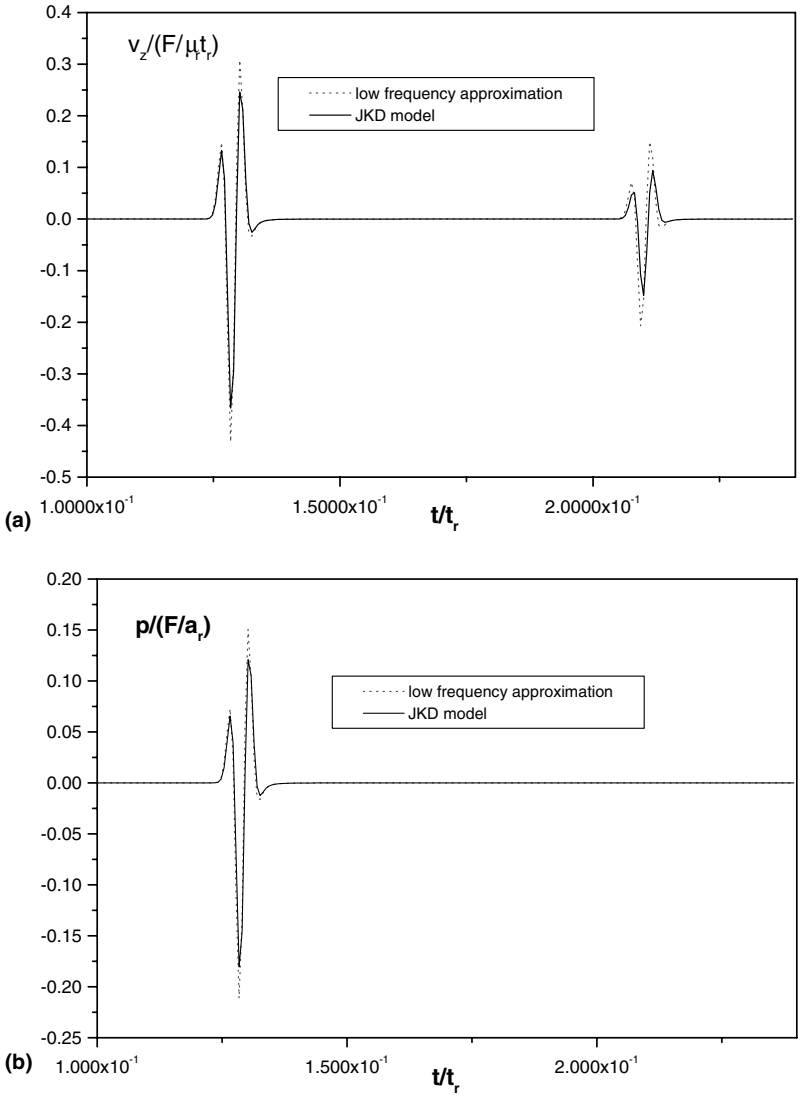

Fig. 1. Comparison between the low-frequency approximation and the JKD model (a) the vertical velocity v_z, (b) the pore pressure p.

$$\dot{v}_z(t) = \frac{m\gamma_s}{\rho_f}(\sigma_{zx,x} + \sigma_{zz,z}) + \gamma_s p_{,z} + \frac{\eta}{k_0}\gamma_s a_s^{-\frac{1}{2}}(D + a_s)^{1/2} q_z + \gamma_s\left(\frac{m}{\rho_f}F_z^b - F_z^f\right), \tag{22b}$$

$$\dot{q}_x(t) = \frac{\rho_f\gamma_f}{\rho}(\sigma_{xx,x} + \sigma_{xz,z}) + \gamma_f p_{,x} + \frac{\eta}{k_0}\gamma_f a_s^{-\frac{1}{2}}(D + a_s)^{1/2} q_x + \gamma_f\left(\frac{\rho_f}{\rho}F_x^b - F_x^f\right), \tag{22c}$$

$$\dot{q}_z(t) = \frac{\rho_f\gamma_f}{\rho}(\sigma_{zx,x} + \sigma_{zz,z}) + \gamma_f p_{,z} + \frac{\eta}{k_0}\gamma_f a_s^{-\frac{1}{2}}(D + a_s)^{1/2} q_z + \gamma_f\left(\frac{\rho_f}{\rho}F_z^b - F_z^f\right), \tag{22d}$$

where $\gamma_s = \rho_f/(m\rho - \rho_f^2)$, $\gamma_f = \rho/(\rho_f^2 - m\rho)$. On the other hand, differentiation of Eq. (12a,b) with respect to time and utilization of Eqs. (13) and (21) yields four first-order differential equations for the stresses and the pore pressure

$$\dot{\sigma}_{xx}(t) = (\lambda + 2\mu + \alpha^2 M)v_{x,x} + (\lambda + \alpha^2 M)v_{z,z} + \alpha M q_{x,x} + \alpha M q_{z,z}, \tag{23a}$$

$$\dot{\sigma}_{zz}(t) = (\lambda + \alpha^2 M)v_{x,x} + (\lambda + 2\mu + \alpha^2 M)v_{z,z} + \alpha M q_{x,x} + \alpha M q_{z,z}, \tag{23b}$$

$$\dot{\sigma}_{zx}(t) = \mu(v_{x,z} + v_{z,x}), \tag{23c}$$

$$\dot{p}(t) = -\alpha M v_{x,x} - \alpha M v_{z,z} - M q_{x,x} - M q_{z,z}. \tag{23d}$$

For the first-order differential equation system of (22) and (23), the following initial conditions are assumed:

$$v_x(0) = 0, \quad v_z(0) = 0, \quad q_x(0) = 0, \quad q_z(0) = 0, \tag{24a–d}$$

$$\sigma_{xx}(0) = 0, \quad \sigma_{zz}(0) = 0, \quad \sigma_{zx}(0) = 0, \quad p(0) = 0. \tag{24e–h}$$

Solving Eqs. (22)–(24) in time domain requires the evaluation of the two shifted fractional derivatives in Eq. (22). In order to show the difficulty encountered in solving Eqs. (22) and (23) by discretizing the shifted fractional derivative directly, we will analyze the shifted fractional derivative operator involved in the drag force $f_x(t)$. In terms of Eq. (14b), $f_x(t)$ has the form

$$f_x(t) = \frac{k_0}{\eta} a_s^{-\frac{1}{2}} (D + a_s)^{1/2} q_x. \tag{25}$$

Using the definition of the Caputo fractional derivative [31] and Eq. (1), Eq. (25) is rewritten as follows:

$$f_x(t) = \frac{k_0}{\eta} a_s^{-\frac{1}{2}} \int_0^t \frac{e^{-a_s(t-\tau)}}{\Gamma(1/2)} (t-\tau)^{-\frac{1}{2}} [a_s q_x(\tau) + \dot{q}_x(\tau)]\, d\tau. \tag{26}$$

It follows from Eq. (26) that $f_x(t)$ depends on the entire history of q_x. Also, the kernel involved in Eq. (26) has a singularity $t^{-1/2}$ at $\tau \to t$, which means that dynamic permeability exhibits a particularly strong dependence on the recent velocity history. Furthermore, the kernel in the convolution of Eq. (26) cannot be approximated by a superposition of a finite number of exponentials (a Prony sum). As a result the convolution cannot be eliminated by introducing internal variables satisfying first-order differential equations [14,15]. Consequently, if Eqs. (22)–(24) are solved in the time domain and the fractional derivatives in Eq. (22) are directly discretized, all the history of the velocities should be stored and integrated, which makes the wave field simulation of the heterogeneous porous medium very expensive.

3. A new method for calculating the fractional derivative $D^{\alpha}\chi(t)$

Before proceeding to solve the differential equations involving shifted fractional derivatives, we shall discuss the calculation of the shifted fractional derivative operator. Up to now, several numerical methods have been proposed for the numerical approximation of the fractional derivative [34,41,42]. The fractional derivative operator also appears in mathematical models of mechanical vibration damping [43–45]. Note that these distributed models are based on the FEM discretization. The main drawback of these methods consists in the necessity of storing and integrating the entire history of the related physical variables. As a result, it is computationally very expensive or impossible to combine these methods with the pseudospectral method to simulate wave motion in the porous medium with singular memory drag force. Recently, Yuan and Agrawal [32] proposed a new numerical approach for calculating the fractional derivative of a function.

The new method does not require integration and storage of the entire history of the function. Unfortunately, as it will be demonstrated below, the Yuan–Agrawal method, which performs well for the discrete mechanical system discussed in their paper, does not yield satisfactory results for the singular dynamic permeability considered here. Hence, in this section, a necessary improvement of the Yuan–Agrawal method for calculating the fractional derivative will be developed.

The key point of Yuan and Agrawal's method is to transform a fractional derivative into an infinite integral over an auxiliary internal variables. Approximating the integral by a specific quadrature formula, the fractional derivative can be evaluated by solving ordinary differential equations for a finite set of quadrature nodes. Following Yuan and Agrawal [32]:

$$D^{\alpha}\chi(t) = \int_0^{+\infty} \phi(y,t)\,\mathrm{d}y, \tag{27a}$$

$$\phi(y,t) = \kappa y^{2\alpha-1}\int_0^t \mathrm{e}^{-(t-\tau)y^2} D\chi(\tau)\,\mathrm{d}\tau, \tag{27b}$$

$$\dot{\phi}(y,t) = -y^2\phi(y,t) + \kappa y^{2\alpha-1} D\chi(t), \tag{27c}$$

where $D := \mathrm{d}/\mathrm{d}t$ and $\kappa = 2\sin(\pi\alpha)/\pi$. Using the Laguerre quadrature formula [46], Eq. (27a) is approximated by the expression

$$D^{\alpha}\chi(t) = \sum_{i=1}^{N} w_i^{(N)} \mathrm{e}^{y_i^{(N)}} \phi(y_i^{(N)}, t), \tag{28a}$$

where the quadrature internal variable $\phi(y_i^{(N)}, t)$ $(i = 1, 2, \ldots, N)$ satisfy the first-order relaxation equations

$$\dot{\phi}(y_i^{(N)}, t) = -y_i^{(N)^2}\phi(y_i^{(N)}, t) + \kappa y_i^{(N)^{2\alpha-1}} D\chi(t), \quad i = 1, 2, \ldots, N, \tag{28b}$$

where N denotes the number of points in the Laguerre quadrature formula. The fractional derivative of $\chi(t)$ can be determined by solving the first-order differential equations for quadrature variables $\phi(y_i^{(N)}, t)$, $i = 1, 2, \ldots, N$ and applying the quadrature formula (28a).

Similar expressions for evaluation the shifted fractional derivative defined by (1) are obtained by the combination of Eq. (27) with Eq. (1) and utilization of the Laguerre quadrature formula

$$(D+\lambda)^{\alpha}\chi(t) = \int_0^{+\infty}\left[\kappa y^{2\alpha-1}\int_0^t \mathrm{e}^{-(t-\tau)y^2-\lambda(t-\tau)}(\lambda\chi(\tau)+\dot{\chi}(\tau))\,\mathrm{d}\tau\right]\mathrm{d}y = \int_0^{+\infty}\phi(y,t)\,\mathrm{d}y, \tag{29a}$$

$$\phi(y,t) = \kappa y^{2\alpha-1}\int_0^t \mathrm{e}^{-(t-\tau)y^2-\lambda(t-\tau)}[\lambda\chi(\tau)+\dot{\chi}(\tau)]\,\mathrm{d}\tau, \tag{29b}$$

$$\dot{\phi}(y,t) = -(y^2+\lambda)\phi(y,t) + \kappa y^{2\alpha-1}[\lambda\chi(t)+\dot{\chi}(t)], \tag{29c}$$

$$(D+\lambda)^{\alpha}\chi(t) = \sum_{i=1}^{N} w_i^{(N)}\mathrm{e}^{y_i^{(N)}}\phi(y_i^{(N)}, t), \tag{29d}$$

$$\dot{\phi}(y_i^{(N)}, t) = -(y_i^{(N)2}+\lambda)\phi(y_i^{(N)}, t) + \kappa y_i^{(N)2\alpha-1}[\lambda\chi(t)+\dot{\chi}(t)], \quad i = 1, 2, \ldots, N. \tag{29e}$$

In terms of Eq. (29), Eq. (25) is reduced to

$$f_x(t) = \frac{k_0}{\eta}a_{\mathrm{s}}^{-\frac{1}{2}}(D+a_{\mathrm{s}})^{1/2}q_x = \frac{k_0}{\eta}a_{\mathrm{s}}^{-\frac{1}{2}}\int_0^{+\infty}\phi(y,t)\,\mathrm{d}y, \tag{30a}$$

$$\phi(y,t) = \kappa y^{2\alpha-1} \int_0^t \mathrm{e}^{-(t-\tau)y^2-(t-\tau)a_\mathrm{s}} [a_\mathrm{s} q_x(\tau) + \dot{q}_x(\tau)]\,\mathrm{d}\tau, \tag{30b}$$

$$\dot{\phi}(y,t) = -(y^2 + a_\mathrm{s})\phi(y,t) + \kappa y^{2\alpha-1}[a_\mathrm{s} q_x(t) + \dot{q}_x(t)], \tag{30c}$$

where $\alpha = 1/2$. For the time being, we assume that the relative velocity $q_x(t)$ is known in advance and has the form of a Ricker wavelet [37]. Obviously, application of the Laguerre quadrature formula to above equation yields the solution of $f_x(t)$ in time domain directly. On the other hand, in terms of Eq. (10), the expression of $f_x(t)$ in the frequency domain has the form

$$\tilde{f}_x(\omega) = \frac{\eta a_\mathrm{s}^{-\frac{1}{2}}}{k_0} (\mathrm{i}\omega + a_\mathrm{s})^{1/2} \mathrm{i}\omega w. \tag{31}$$

Therefore, alternatively, the solution of $f_x(t)$ in time domain can also be recovered by applying the FFT (fast Fourier transform) to Eq. (31). In numerical calculations, $\omega_\mathrm{T} = 1000\ \mathrm{s}^{-1}$, $K = 0.5$, N in Eq. (29) is taken as 25 and ω_c, t_s in Eq. (16) are taken as $400\pi\ \mathrm{s}^{-1}$ and 0.01 s, respectively. The drag force $f_x(t)$ calculated by Eqs. (30) and by the FFT method is shown in Fig. 2(a). It follows from Fig. 2(a) that there are significant differences between the two solutions.

The reason for this shortcoming is the slow convergence of the quadrature formula which is due to singularity of the integrand. However, the convergence can be improved by using a more accurate quadrature formula to evaluate the infinite integral of Eq. (29a). To this effect we consider the asymptotic behavior of Eq. (29b). When y tends to zero, the asymptotic expression of $\phi(y,t)$ is

$$\phi(y,t) \overset{y\to 0}{\approx} \kappa y^{2\alpha-1} \int_0^t \mathrm{e}^{-\lambda(t-\tau)} [\lambda\chi(\tau) + \dot{\chi}(\tau)]\,\mathrm{d}\tau. \tag{32}$$

On the other hand, the asymptotic expression for $\phi(y,t)$ when y tends to infinity has the following form:

$$\phi(y,t) \overset{y\to\infty}{\approx} \kappa y^{2\alpha-3}[\lambda\chi(t) + \dot{\chi}(t)]. \tag{33}$$

In terms of Eqs. (32) and (33), one can conclude that when α tends to zero or one, the infinite integral in Eq. (29a) will converge very slowly. Consequently, in this case, the Laguerre integral formula is not an efficient way to evaluate (29a). In order to accelerate the convergence of the infinite integral, Eq. (29a) is rewritten in the following form:

$$\begin{aligned}(D+\lambda)^\alpha \chi(t) &= \int_0^{+\infty} \phi(y,t)\,\mathrm{d}y \\ &= \int_0^c \phi(y,t)\,\mathrm{d}y + \int_\mathrm{c}^{+\infty} [\phi(y,t) - \kappa y^{2\alpha-3}(\lambda\chi(t) + \dot{\chi}(t))]\,\mathrm{d}y + \kappa \int_\mathrm{c}^{+\infty} y^{2\alpha-3}[\lambda\chi(t) + \dot{\chi}(t)]\,\mathrm{d}y,\end{aligned} \tag{34}$$

where c is a constant. In order to take into account the singularity at $y = 0$, the first integral is evaluated by Gauss–Jacobi quadrature formula [46]. Obviously, the second integral in the above equation converges much faster than the original one. Moreover, the third integral can be evaluated in closed form. Using the Gauss–Jacobi quadrature formula [46] to calculate the first integral and the shifted Laguerre integral formula to calculate the second integral and calculating the third integral in the above equation, one has

$$(D+\lambda)^\alpha \chi(t) = \sum_{i=1}^{n_\mathrm{G}} w_i^{(n_\mathrm{G})} \phi(y_i^{(n_\mathrm{G})}, t) + \sum_{i=1}^{n_\mathrm{L}} w_i^{(n_\mathrm{L})} \phi(y_i^{(n_\mathrm{L})}, t) + \Psi_\mathrm{L}[\lambda\chi(t) + \dot{\chi}(t)], \tag{35}$$

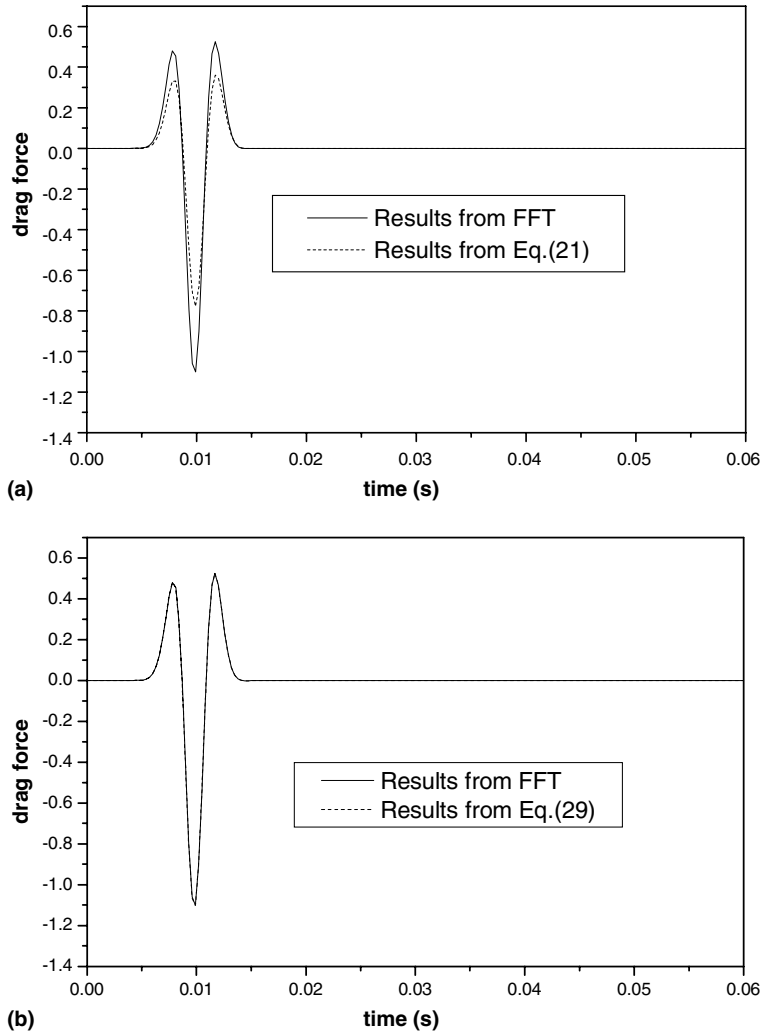

Fig. 2. Comparison between the solutions of drag force by the fractional derivative method and the FFT method (a) the Yuan–Agrawal method and the FFT method, (b) the improved Yuan–Agrawal method and the FFT method.

where n_G, n_L are number of quadrature points for the Gauss–Jacobi quadrature formula and the shifted Laguerre integral formula respectively, $y_i^{(n_G)}$ $(i = 1, 2, \ldots, n_G)$, $w_i^{(n_G)}$ $(i = 1, 2, \ldots, n_G)$ and $y_i^{n_L}$ $(i = 1, 2, \ldots, n_L)$, $w_i^{n_L}$ $(i = 1, 2, \ldots, n_L)$ are the corresponding abscissas and quadrature weights. In addition, Ψ_L is given by

$$\Psi_L = \kappa \left[\frac{c^{2\alpha-2}}{2-2\alpha} - \sum_{i=1}^{n_L} w_i^{(n_L)} \left(y_i^{(n_L)}\right)^{2\alpha-3} \right]. \tag{36}$$

Combination of the first two terms in Eq. (35) yields

$$(D+\lambda)^{\alpha}\chi(t) = \sum_{i=1}^{N_I} w_i \phi(y_i, t) + \Psi_L[\lambda\chi(t) + \dot{\chi}(t)], \tag{37a}$$

$$w_i = \begin{cases} w_i^{(n_G)}, & i \leqslant n_G, \\ w_{i-n_G}^{(n_L)}, & i > n_G, \end{cases} \quad i = 1, 2, \ldots, N_I, \qquad y_i = \begin{cases} y_i^{(n_G)}, & i \leqslant n_G, \\ y_{i-n_G}^{(n_L)}, & i > n_G, \end{cases} \quad i = 1, 2, \ldots, N_I, \tag{37b, c}$$

where $N_I = n_G + n_L$. Obviously, the above regularization of the integral (29a) accelerates its convergence and more importantly, accounts for the singularity at $y = 0$ and $y = \infty$.

The quadrature formula for fractional derivative operator has been improved and a new quadrature formula Eq. (37) for the fractional derivative operator has been derived. For a numerical test of the proposed quadrature formula, again, the drag force (25) is calculated by using Eq. (37) and the same parameters as above. In calculation, $n_G = 10$, $n_L = 15$ and $c = 1.0$. Again, the numerical results obtained by Eq. (37) are compared with the results obtained by the FFT method. Fig. 2(b) shows clearly that the results obtained by the two methods agree very well. Therefore, in this section, a new general method for calculating the fractional derivative has been developed. The new approach has the following advantages. First, for evaluating of present solution, the storage and integration of the entire histories of variables are not needed. Moreover, the method yields sufficiently accurate results for a fractional derivative of an order $0 < \alpha < 1$ by using a relatively small number of quadrature points, which is crucial for reducing the computational cost of the scheme to an acceptable level.

4. Numerical scheme for the two-dimensional saturated porous medium

2D wave propagation in a saturated porous medium with the JKD dynamic permeability is described by Eqs. (22) and (23) together with the initial condition (24). For the four equations of (22) involving shifted fractional derivative operators, the method developed in the last section will be applied. In this way, the four ordinary differential equations will be reduced to four ordinary differential equations supplemented by the ordinary differential equations for the quadrature variables associated with the drag force. The first-order ordinary differential equations for the velocity, stress and pore pressure together with those for the quadrature variables constitute the differential equations system for the porous medium. The Fourier pseudospectral method is used to calculate the horizontal and vertical spatial derivatives. Moreover, the differential equation system is propagated in time by a predictor–corrector method.

4.1. Differential equations for the two-dimensional porous medium in matrix form

Combining Eq. (37) with Eq. (22) and using Eqs. (23) and (24), the matrix form first-order differential equations for all the variables are obtained as follows:

$$\frac{\partial \mathbf{V}}{\partial t} = \mathbf{A}\frac{\partial \mathbf{V}}{\partial x} + \mathbf{B}\frac{\partial \mathbf{V}}{\partial z} + \mathbf{C}, \quad \mathbf{V}(0) = \mathbf{0}, \tag{38a, b}$$

where

$$\mathbf{V} = \left[v_x, v_z, q_x, q_z, \sigma_{xx}, \sigma_{zz}, \sigma_{zx}, p, \langle \phi^x_{i=1,\ldots,N_I} \rangle_{N_I}, \langle \phi^z_{i=1,\ldots,N_I} \rangle_{N_I}\right]^T, \tag{38c}$$

where $v_x, v_z, q_x, q_z, \sigma_{xx}, \sigma_{zz}, \sigma_{zx}, p$ are the velocity, stress and pore pressure of the two-dimensional porous medium; while ϕ_i^x, ϕ_i^z, $i = 1, 2, \ldots, N_I$ are the quadrature variables associated with the drag force in x, z directions and $\langle \bullet \rangle_{N_I}$ denotes a set of N_I elements; $\mathbf{A}$, $\mathbf{B}$ are $(2N_I + 8) \times (2N_I + 8)$ matrices and $\mathbf{C}$ is $(2N_I + 8) \times 1$ matrix. As the matrices $\mathbf{A}$, $\mathbf{B}$, $\mathbf{C}$ can be derived by (22), (23) and (37) in a rather straightforward way, hence, the entries of the matrices $\mathbf{A}$, $\mathbf{B}$, $\mathbf{C}$ are omitted here.

4.2. Spatial discretization by the Fourier pseudospectral method

As mentioned above, for the horizontal and vertical derivatives involved in the governing equation (38), the Fourier pseudospectral method [47] which include spatial discretization as well as the calculation of spatial derivative by fast Fourier transformation (FFT) is used. In this paper, the discrete Fourier transform (DFT) and inverse discrete Fourier transformation (IDFT) are defined as follows [48]:

$$H_n := \sum_{k=0}^{N-1} h_k \mathrm{e}^{-2\pi \mathrm{i} kn/N}, \quad h_k := \frac{1}{N} \sum_{n=0}^{N-1} H_n \mathrm{e}^{2\pi \mathrm{i} kn/N}, \tag{39a, b}$$

where h_k, $k = 0, 1, 2, \ldots, N-1$ and H_n, $n = 0, 1, 2, \ldots, N-1$ are N sample values in the spatial domain and in the transformed domain, respectively.

In the calculation direction the coordinates of the sampling points are given by

$$x_k = \Delta x(k-1), \quad k = 1, 2, \ldots, N_x, \quad \Delta x = \frac{x_{\max}}{N_x - 1}, \tag{40a, b}$$

where $x_{\max}$ is the maximum distance in the calculation direction and N_x is the number of the grid points in the calculation direction, Δx is the mesh size. Note that the period of fast Fourier transform (FFT) in the calculation direction is equal to $x_{\max} + \Delta x$. Moreover, due to the Hermitean property of the derivative, the N_x in the above equation should be an odd number [47]. Obviously, if N_x is even, the DFT as shown in Eq. (39) has a Nyquist component and the corresponding derivative loses the Hermitean property. In terms of the definition of DFT in Eq. (39), for a given function $f(x)$ with the transformed function $\tilde{f}(k_x)$, the derivative of $f(x)$ is calculated by

$$\frac{\mathrm{d}\tilde{f}}{\mathrm{d}x} = \mathrm{i}k_x \tilde{f}(k_x), \tag{41a}$$

$$k_x = (j-1)\Delta k_x, \quad j \leqslant \frac{N_x + 1}{2}, \quad k_x = -(N_x - j + 1)\Delta k_x, \quad j > \frac{N_x + 1}{2}, \tag{41b, c}$$

$$\Delta k_x = \frac{2\pi}{N_x \Delta x}, \quad j = 1, 2, \ldots, N_x, \tag{41d}$$

where $\mathrm{i} = \sqrt{-1}$.

Since the spatial differentiation of the equation of motion is implemented by the FFT method, a wrap-around effect may appear. Also, the unbounded domain is simulated by a finite domain with boundary. Thus, the reflection from the non-physical boundary should be avoided. Therefore, an absorbing region is added along the computational domain to prevent wrap-around and non-physical reflection [49].

5. Numerical results

In order to verify the proposed approach, the first example simulates the wave field of a point force applied in an unbounded homogeneous 2D porous medium with the JKD model. Our results from the pseudospectral method are compared with the results obtain by the potential method. In the second example, the wave field of a 2D porous medium with Biot's parameter M increasing linearly with depth will be calculated. In the third example, the wave field of a porous medium constituted of two layers with the lower layer containing one rectangular inclusion is calculated.

5.1. Example A: an unbounded 2D porous medium subject to a point force

In this example, the wave propagation in a 2D homogenous porous full plane with the JKD model is simulated. Our results from the Fourier pseudospectral method are compared with those from potential method as shown in Section 2.

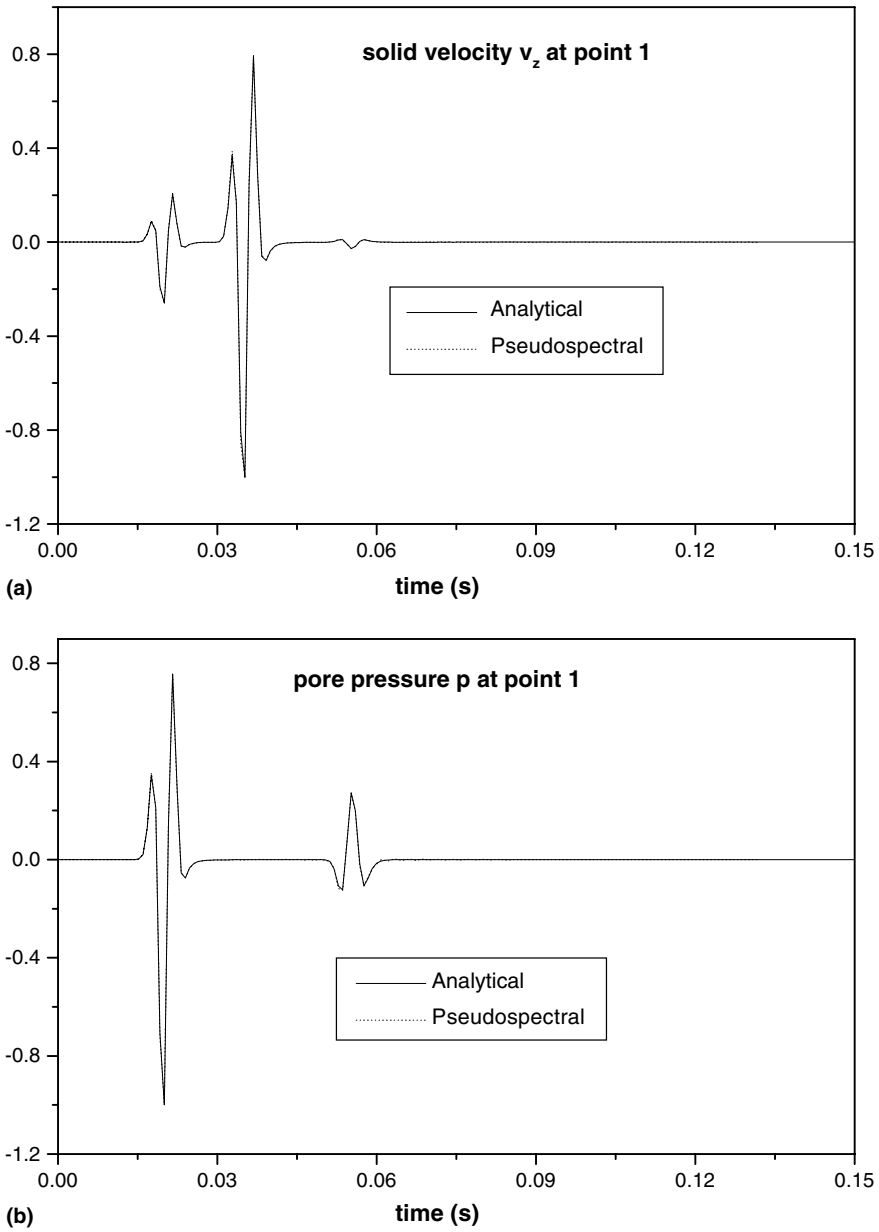

Fig. 3. Comparison of results at point 1 by the pseudospectral method and by the analytical method (a) solid velocity v_z at point 1, (b) pore pressure p at point 1.

In this example, the parameters for the porous medium are as follows: $\rho_f = 1.0 \times 10^3$ kg/m^3, $\rho_s = 2.0 \times 10^3$ kg/m^3, $\phi = 0.3$, $\lambda = 1.0 \times 10^9$ Pa, $\mu = 2.0 \times 10^9$ Pa, $\alpha = 0.9$, $M = 1.0 \times 10^{10}$ Pa, $\eta = 1.0 \times 10^{-3}$ Pa s, $k_0 = 4.0 \times 10^{-9}$ m^2, $a_\infty = 3.0$, $K = 0.5$. Note that in order to ensure visibility of the P_2 wave and also for a thorough test of our method, the parameter k_0 is larger than the normal values. Since the calculation domain is homogeneous, $n_G = 5$, $n_L = 20$ and $c = 1.0$ are used for all the grids. In calculation, a numerical grid

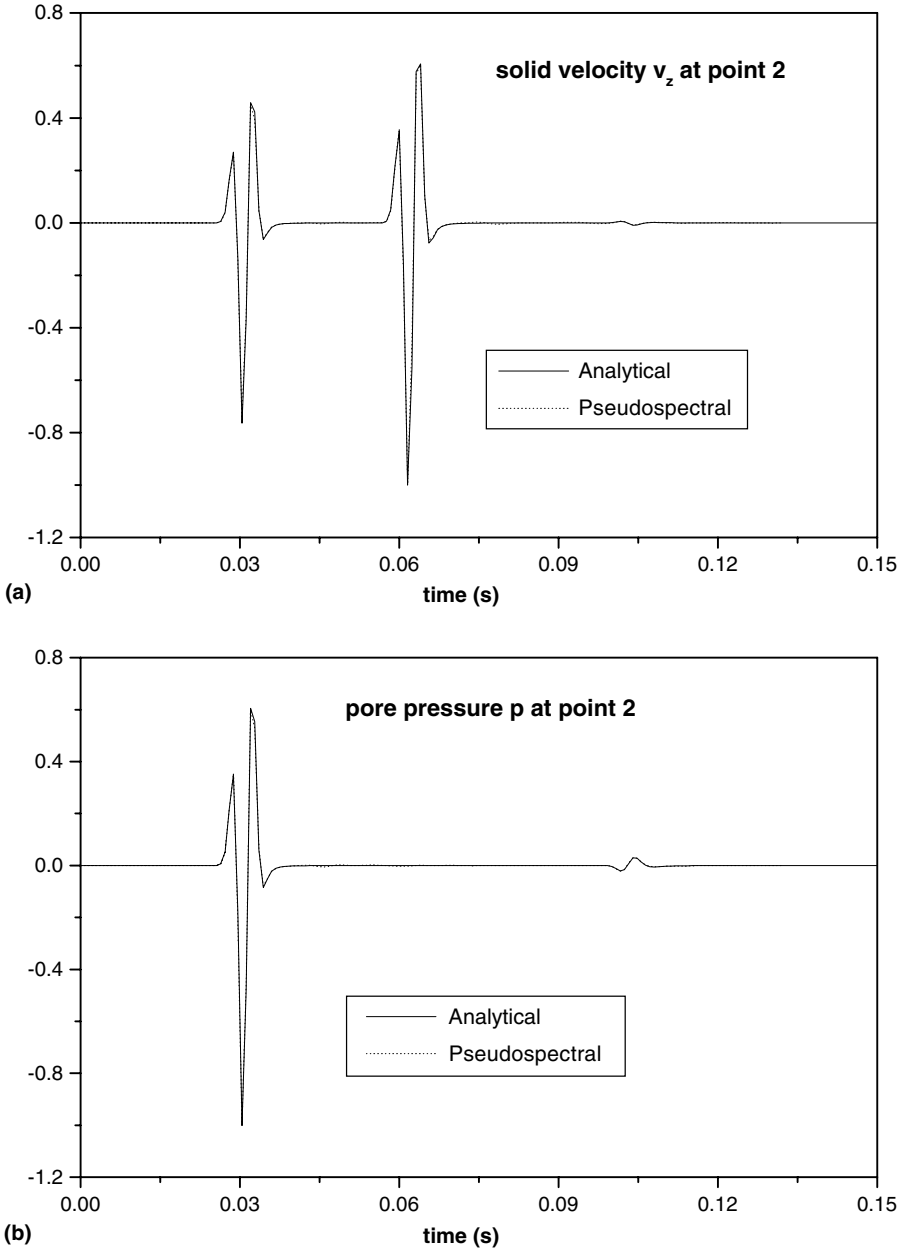

Fig. 4. Comparison of results at point 2 by the pseudospectral method and the analytical method (a) solid velocity v_z at point 2, (b) pore pressure p at point 2.

$N_x \times N_z = 141 \times 141$ with $\Delta x = 1.0$ m and $\Delta z = 1.0$ m is used. The dimensions of physical domain are $x_{\max} = 140$ m, $z_{\max} = 140$ m. Moreover, in order to prevent the non-physical reflection and wrap-around, absorbing strips of length 20 grid points are used around the calculation domain. The source is the vertical force applied in the solid skeleton and the signal is a Ricker wavelet with $\omega_c = 400\pi\ s^{-1}$ and $t_s = 0.01$ s. The vertical point force is located at $(x, z) = (40\,\text{m}, 39\,\text{m})$ with grid number $(I_x, I_z) = (41, 40)$ where I_x, I_z denote the grid number in the horizontal direction and vertical direction, respectively. The first receiver (point 1) is located at $(x, z) = (60\,\text{m}, 59\,\text{m})$ with grid number $(I_x, I_z) = (61, 60)$, while the second receiver (point 2) is located at $(x, z) = (70\,\text{m}, 89\,\text{m})$ with grid number $(I_x, I_z) = (71, 90)$. The governing equations (38) are solved over the time range 0.132 s with a time step of 4.0×10^{-5} s by using a second-order predictor–corrector method. In Figs. 3 and 4, the plots of v_z, p for the two receivers obtained by the FFT method and by the pseudospectral method are compared. It follows from Figs. 3 and 4 that the agreement between the FFT method and the pseudospectral method is quite good. Figs. 3 and 4 show that the P_2 wave has a more

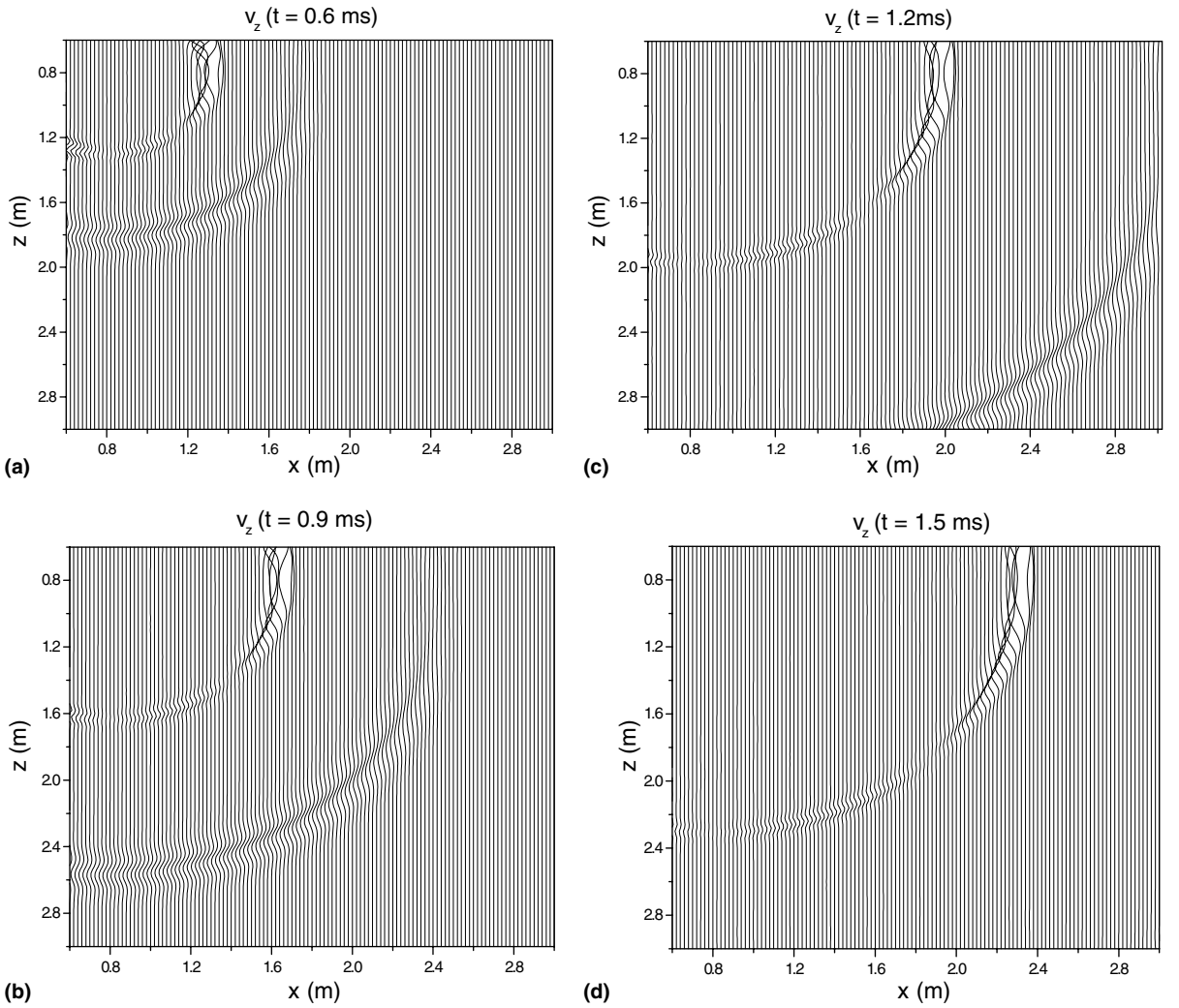

Fig. 5. Snapshots of solid velocity v_z in Example B (a) v_z for $t = 0.6$ ms, (b) v_z for $t = 0.9$ ms, (c) v_z for $t = 1.2$ ms, (d) v_z for $t = 1.5$ ms.

obvious influence on p than on v_z. Besides, due to attenuation, compared with the point 1, the amplitudes of the P_2 wave at the point 2 is smaller.

5.2. Example B: the porous medium with Biot's parameter M increasing linearly with depth

This example consider the porous medium with linear variation of Biot's parameter M with increasing depth. The dimensions of the physical space are $x_{\max} = 3.6$ m and $z_{\max} = 3.6$ m. For the numerical calculation, a numerical grid $N_x \times N_z = 181 \times 181$ with $\Delta x = \Delta z = 2.0 \times 10^{-2}$ m is used. In order to eliminate the non-physical reflections and the wrap-around, absorbing strips of 30 grids are used at each side of the calculation domain. The parameters for the porous medium are as follows: $\rho_f = 1.0 \times 10^3$ kg/m^3, $\rho_s = 2.0 \times 10^3$ kg/m^3, $\phi = 0.3$, $\lambda = 1.0 \times 10^9$ Pa, $\mu = 2.0 \times 10^9$ Pa, $\alpha = 0.9$, $\eta = 1.0 \times 10^{-3}$ Pa s, $k_0 = 5.0 \times 10^{-12}$ m^2,

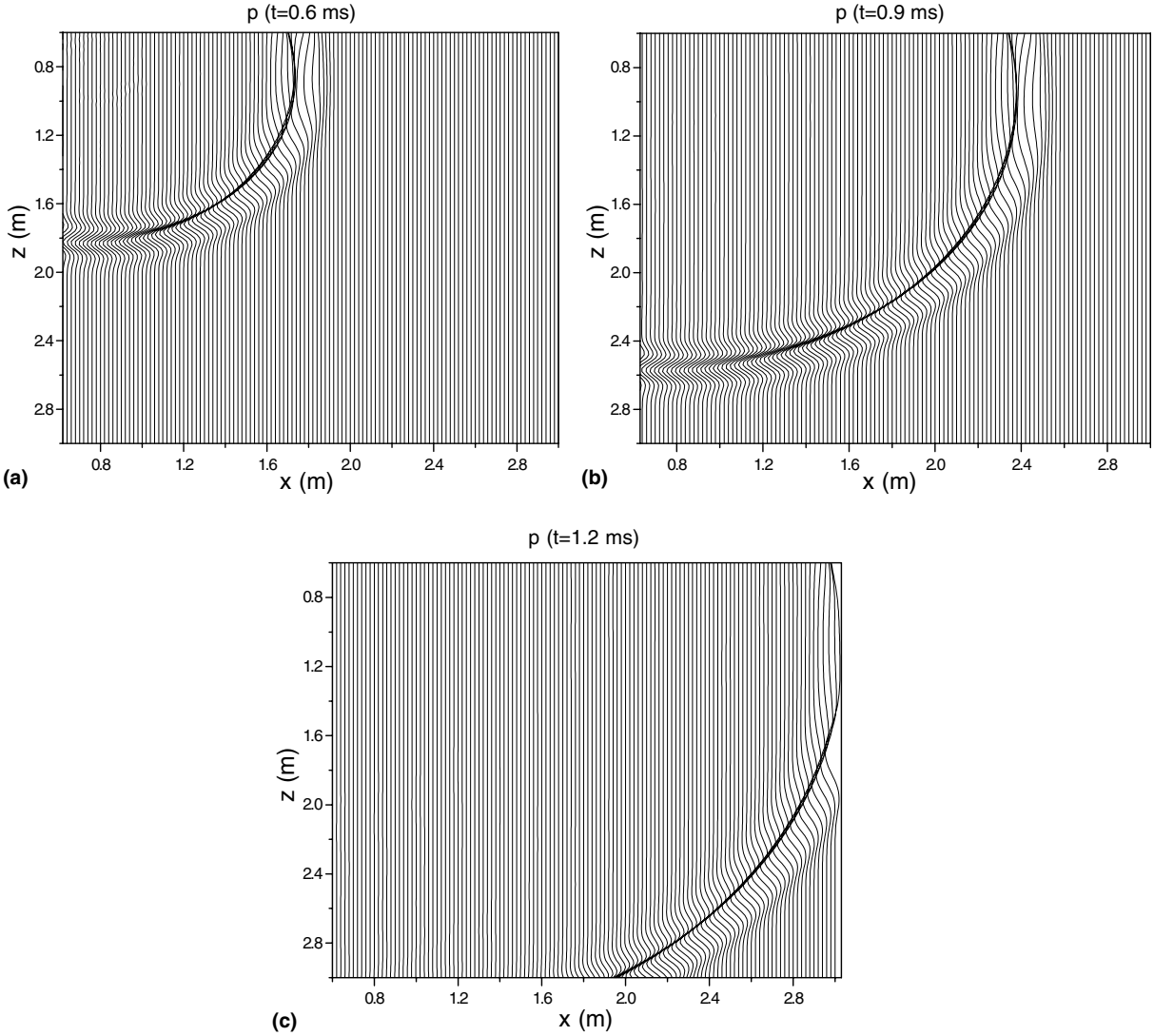

Fig. 6. Snapshots of pore pressure p in Example B (a) p for $t = 0.6$ ms, (b) p for $t = 0.9$ ms, (c) p for $t = 1.2$ ms.

$a_\infty = 3.0$, $K = 0.5$. In calculation, $n_G = 5$, $n_L = 20$ and $c = 5.0$ are used for all the grids. Biot's parameter M varies linearly along the vertical direction and is given by the following formula:

$$M(z) = M(0) + \left[(M(z_{\max}) - M(0)) \frac{z}{z_{\max}} \right], \tag{42}$$

where $M(0)$, $M(z_{\max})$ are Biot's parameter M for the top and the bottom grid of the calculation domain and $M(0) = 1.25 \times 10^9$ Pa, $M(z_{\max}) = 1.0 \times 10^{10}$ Pa. The source is a point force applied at the solid skeleton. The point force is oriented at 45° oblique angle with respect to the vertical direction and emits a Ricker signal with $f_c = 1.0 \times 10^4$ Hz and $t_s = 1.5 \times 10^{-4}$ s, respectively. The force is applied at the point with the grid number $(I_x, I_z) = (41, 41)$. The calculation is carried out for a total propagation time of 3.0×10^{-3} s with a time step of 1.0×10^{-6} s by a second-order predictor–corrector method.

Figs. 5(a)–(d) show the snapshots of the vertical velocity v_z at time 0.6, 0.9, 1.2 and 1.5 ms. Figs. 6(a)–(c) show the snapshots of the pore pressure p at time 0.6, 0.9, and 1.2 ms. In Figs. 5 and 6, due to attenuation, no P_2 wave is visible. Fig. 6 shows that the pore pressure is not related to the S wave, which agrees with Biot's theory. Besides, Figs. 5 and 6 show that the P_1 wave front propagates over a longer distance in the vertical direction than in the horizontal direction, while the S wave propagates the same distances in both directions. This also agrees with Biot's theory, as in terms of Biot's theory, Biot's parameter M only affect the speed of the P wave. Moreover, Fig. 6 shows clearly that due to the increasing of Biot's parameter M in vertical direction, the pore pressure p in the wave front of vertical direction are larger than those of the horizontal direction.

5.3. Example C: two porous layers and a rectangular inclusion

In this example, a two-layer porous medium is considered. The bottom layer contains a rectangular inclusion. The dimensions of the physical space are $x_{\max} = 3.2$ m and $z_{\max} = 4.0$ m. For numerical calculation, a grid size 161 in the horizontal direction and 201 in the vertical direction with $\Delta x = \Delta z = 2.0 \times 10^{-2}$ m are used. In order to eliminate the non-physical reflections and wrap-around, absorbing strips of 30 grids are used on each side of the calculation domain. The top porous layer stretches from grid point 1 to 81 in the vertical direction, while the bottom layer ranges between the grid point 82 and 201 in the vertical direction. The inclusion in the bottom porous layer is located at $I_x \times I_z = [66, 96] \times [112, 142]$ (Fig. 7). The elastic

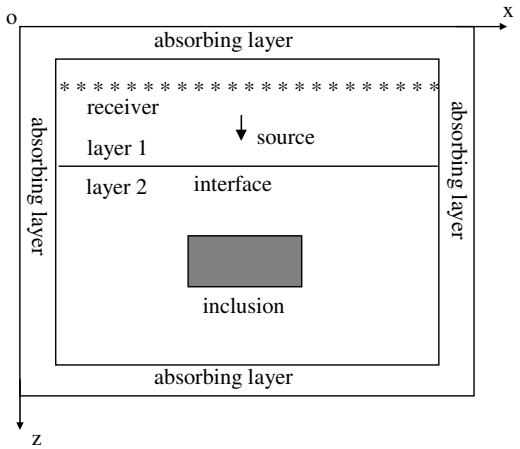

Fig. 7. Two porous layers with the lower layer containing one rectangular inclusion.

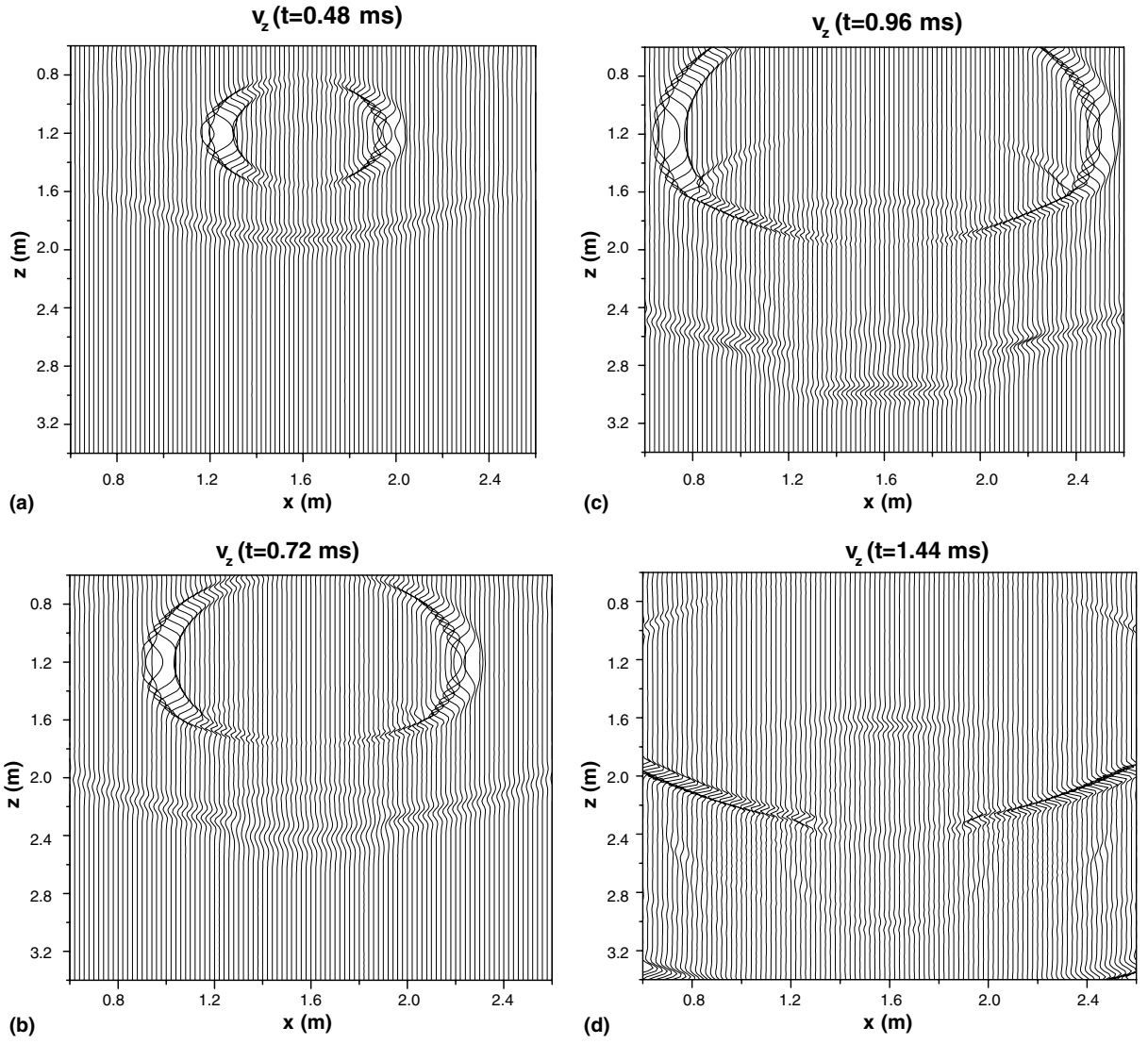

Fig. 8. Snapshots of solid velocity v_z in Example C (a) v_z for $t = 0.48$ ms, (b) v_z for $t = 0.72$ ms, (c) v_z for $t = 0.96$ ms, (d) v_z for $t = 1.44$ ms.

parameters of the top and bottom layer are $\lambda_1 = 1.0 \times 10^9$ Pa, $\mu_1 = 2.0 \times 10^9$ Pa, $M_1 = 1.0 \times 10^{10}$ Pa and $\lambda_2 = 5.0 \times 10^8$ Pa, $\mu_2 = 1.0 \times 10^9$ Pa, $M_2 = 3.0 \times 10^9$ Pa, respectively. The elastic parameters λ_i, μ_i, M_i of the inclusion take the same values as the top layer. The remaining parameters are the same for the top, the bottom layer and the inclusion and are given as follows: $\rho_f = 1.0 \times 10^3$ kg/m^3, $\rho_s = 2.0 \times 10^3$ kg/m^3, $\phi = 0.3$, $\alpha = 0.9$, $\eta = 1.0 \times 10^{-3}$ Pa s, $k_0 = 5.0 \times 10^{-12}$ m^2, $a_\infty = 3.0$, $K = 0.5$. In calculation, $n_G = 5$, $n_L = 20$ and $c = 5.0$ are used for all the grids in the layered porous medium. The calculation is carried out for a total propagation time of 2.4×10^{-3} s with a time step of 0.80×10^{-6} s by a second-order predictor–corrector method. The source is a vertical point force applied in the solid skeleton and emitting the Ricker wavelet

with $f_c = 1.0 \times 10^4$ Hz and $t_s = 1.5 \times 10^{-4}$ s. The location of the vertical point force is $(x, z) = (1.6\,\mathrm{m}, 1.2\,\mathrm{m})$ corresponding to the grid number $(I_x, I_z) = (81, 61)$.

Figs. 8(a)–(d) give the snapshots of the vertical velocity v_z at time 0.48, 0.72, 0.96 and 1.44 ms. Figs. 9(a)–(d) present the snapshots of the stress σ_{zz} at time 0.48, 0.72, 0.96 and 1.44 ms, while Figs. 10(a)–(d) show the snapshots of the pore pressure p at time 0.48, 0.72, 0.96 and 1.44 ms. At time 0.48 ms, the direct P_1 and S wave appear in the upper layer. Also, the reflected P_1 wave is visible in the snapshots of the stress and pore pressure. Besides, in the snapshot of pore pressure at time 0.48 ms, the P_2 wave appears but with relatively smaller amplitude. Note that for the vertical velocity v_z, the contributions from the P_1 wave are much smaller than those from S wave. At time 0.72 ms, the direct P_1 wave is outside the calculation domain while the reflected P_1 wave is at the edge of the domain. The direct S wave dominates in the upper layer. Also,

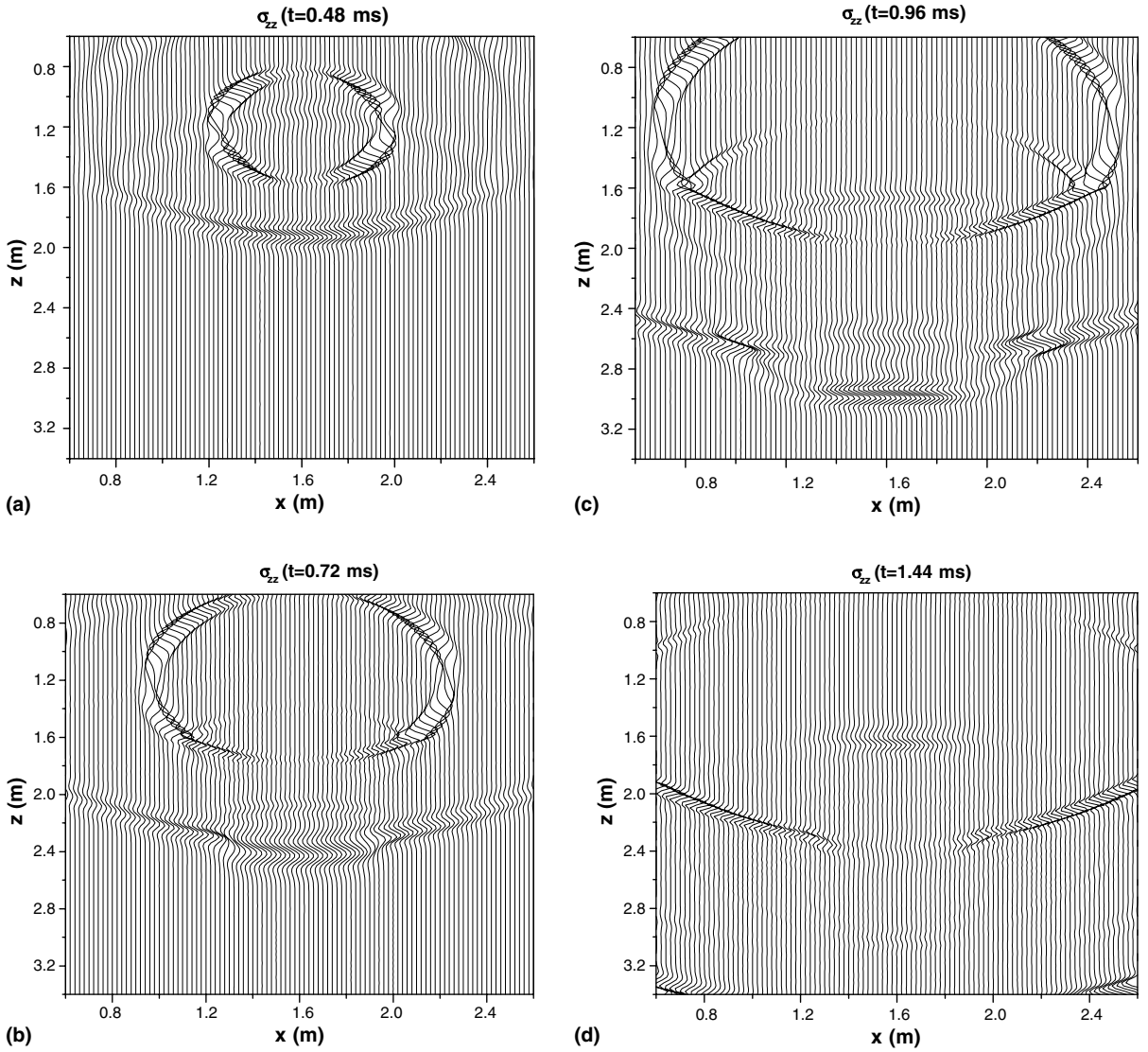

Fig. 9. Snapshots of stress σ_{zz} in Example C (a) σ_{zz} for $t = 0.48$ ms, (b) σ_{zz} for $t = 0.72$ ms, (c) σ_{zz} for $t = 0.96$ ms, (d) σ_{zz} for $t = 1.44$ ms.

the reflected P_1 wave of the direct S wave can be observed. In the lower layer, the transmitted P_1 wave of the direct P_1 dominates. Moreover, the transmitted P_1 wave in the lower layer due to the direct S wave is visible. In the lower layer, the reflected P_1 wave from the upper boundary of the inclusion can also be observed. The P_2 wave, which was observed in the snapshot of pore pressure at 0.48 ms, is invisible at time 0.72 ms due to high attenuation. At time 0.96 ms, in the upper layer neither the direct P_1 wave nor the reflected P_1 wave can be seen. The direct S wave and the reflected S wave propagate in the upper layer. In the lower layer, the transmitted P_1 wave and S wave due to the direct S wave in the upper layer can be seen. The P_1 reflection of the transmitted P_1 wave from the upper boundary of the inclusion can also be observed. Moreover, the transmitted P_1 wave in the lower layer is visible below the inclusion. It is worth noting that in Figs. 9(c) and 10(c), the reflected P_1 wave inside the inclusion can be seen. In time 1.44 ms, in the upper layer, only

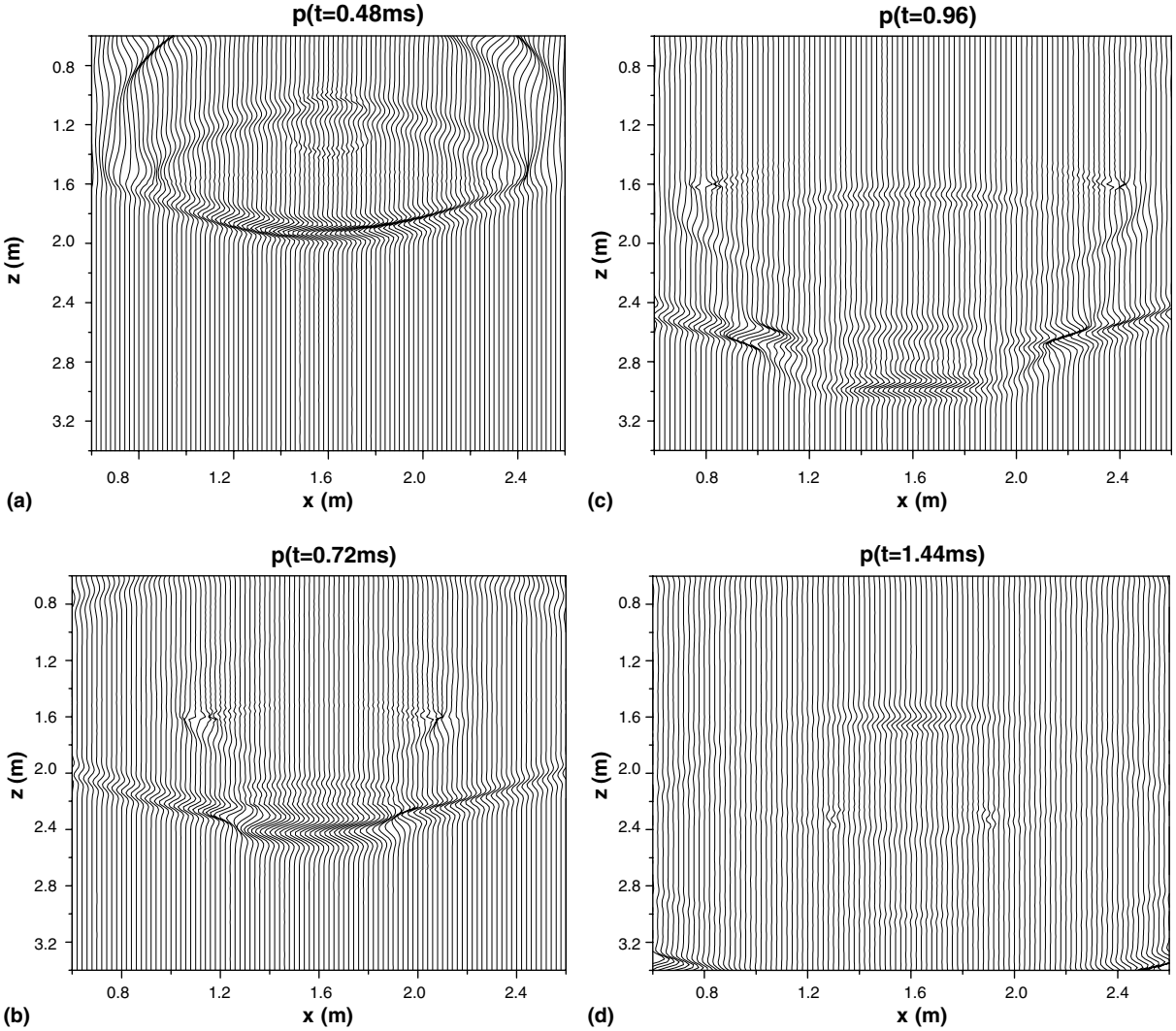

Fig. 10. Snapshots of pore pressure p in Example C (a) p for $t = 0.48$ ms, (b) p for $t = 0.72$ ms, (c) p for $t = 0.96$ ms, (d) p for $t = 1.44$ ms.

the reflected wave due to direct S wave from the layer interface remains. In the lower layer, the transmitted P_1 wave is at the edge of the domain, and the transmitted S wave propagates in the middle of the lower layer. Besides, the reflected P_1 wave from the upper boundary of the inclusion also appears. Moreover, the transmitted S wave in the lower layer is much less affected by the inclusion than by the lower layer.

6. Conclusions

A new method for modeling wave propagation in a porous medium with the JKD model has been developed. The drag force in the JKD model is expressed in terms of the shifted fractional derivative of the relative fluid velocity. A new method for the calculation of the fractional derivative has been developed and applied in solving the differential equations involving shifted fractional derivatives. The new method is also of importance for other applied engineering sciences involving fractional derivatives. The new method of calculating fractional derivatives avoids storage and integration of the entire variable histories in wave field simulation. Thus, our approach is more economical than the methods based on a direct discretization of the fractional derivative. Moreover, the combination of the new method for calculating fractional derivative with the Fourier pseudospectral methods makes our method very efficient in terms of computer storage, due to the fact that the Fourier pseudospectral method is accurate up to the maximum wave number of the mesh that corresponds to a spatial wavelength of two grid points. Also, extension of our method to the three-dimensional wave propagation is straightforward. Furthermore, material anisotropy can be easily incorporated in our method.

Acknowledgments

The research is financed by the Norwegian Scientific Council in the framework of the Petroforsk Project 149238/431 ''Mathematical formulation of seismic attenuation based on physical models of mechanical rock behavior''. Also, the valuable comments from three anonymous reviewers are greatly acknowledged.

References

[1] MA. Biot, Theory of propagation of elastic waves in a fluid-saturated porous solid, I, low frequency range, J. Acoust. Soc. Am. 28 (1956) 168–178.
[2] M.A. Biot, Theory of propagation of elastic waves in a fluid-saturated porous solid, II: Higher frequency range, J. Acoust. Soc. Am. 28 (1956) 179–191.
[3] M.A. Biot, Mechanics of deformation and acoustic propagation in porous medium, J. Appl. Phys. 33 (1962) 1482–1498.
[4] J. Plona, Observation of a second bulk compressional wave in a porous medium at ultrasonic frequency, Appl. Phys. Lett. 36 (1980) 259–261.
[5] J.P. Jones, Raleigh waves in porous elastic fluid saturated solid, J. Acoust. Soc. Am. 33 (1961) 959–962.
[6] H. Deresiewicz, The effect of boundaries on wave propagation in a liquid filled porous solid: IV. Surface waves in a half-spaces, Bull. Seism. Soc. Am. 52 (1962) 627–638.
[7] H. Deresiewicz, R. Skalak, On the uniqueness in dynamic poroelasticity, Bull. Seism. Soc. Am. 53 (1963) 783–788.
[8] T. Senjuntichai, R.K.N.D. Rajapakse, Dynamic Green's functions of homogeneous poroelastic half-plane, J. Eng. Mech. ASCE 120 (1994) 2381–2464.
[9] A.N. Norris, Radiation from a point source and scattering theory in a fluid-saturated porous solid, J. Acoust. Soc. Am. 77 (1985) 2012–2023.
[10] C. Zimmerman, M. Stern, Boundary-element solution of 3-D wave scatter problems in a poroelastic medium, Eng. Anal. Bound. Elem. 12 (1993) 223–240.
[11] A. Hanyga, M.G. Seredynska, Asymptotic ray theory in poro- and viscoelastic media, Wave Motion 30 (1999) 175–195.
[12] A. Hanyga, Asymptotic Green's functions in poroelasticity, J. Comp. Acoust. 11 (2003) 491–501.

[13] T. Ozdenvar, G.A. McMechan, Algorithms for staggered-grid computations for poroelastic, elastic, acoustic, and scalar wave equations, Geophys. Prospecting 45 (1997) 403–420.
[14] J.M. Carcione, Wave propagation in anisotropic, saturated porous media: plane-wave theory and numerical simulation, J. Acoust. Soc. Am. 99 (1996) 2655–2666.
[15] J.C. Simo, T.J.R. Hughes, Computational Inelasticity, Springer, New York, 1998.
[16] D.L. Johnson, J. Koplik, R. Dashen, Theory of dynamic permeability and tortuosity in fluid-saturated porous-media, J. Fluid Mech. 176 (1987) 379–402.
[17] S.R. Pride, F.D. Morgan, A.F. Gangi, Drag forces of porous-medium acoustics, Phys. Rev. B 47 (1993) 4964–4978.
[18] D.K. Wilson, Simple, relaxational models for the acoustical properties of porous media, Appl. Acoust. 50 (1997) 171–188.
[19] D.K. Wilson, Relaxation-matched modeling of propagation through porous-media, including fractal pore structure, J. Acoust. Soc. Am. 94 (1993) 1136–1145.
[20] Y. Champoux, M.R. Stinson, On acoustical models for sound-propagation in rigid frame porous materials and the influence of shape factors, J. Acoust. Soc. Am. 92 (1992) 1120–1131.
[21] S.R. Pride, J.G. Berryman, J.M. Harris, Seismic attenuation due to wave-induced flow, J. Geophys. Res. 109 (2004) B01201.
[22] B. Gurevich, S.L. Lopatnikov, Velocity and attenuation of elastic-waves in finely layered porous rocks, Geophys. J. Int. 121 (1995) 933–947.
[23] S. Gelinsky, S.A. Shapiro, T. Muller, B. Gurevich, Dynamic poroelasticity of thinly layered structures, Int. J. Solids Struct. 35 (1998) 4739–4751.
[24] S.A. Shapiro, T.M. Muller, Seismic signatures of permeability in heterogeneous porous media, Geophysics 64 (1999) 99–103.
[25] M. Batzle, R. Hofmann, D.-H. Han, J. Castagna, Fluids and frequency dependent seismic velocity of rocks, The Leading Edge 20 (2001) 168–171.
[26] S.K. Chang, H.L. Liu, D.L. Johnson, Low-frequency tube waves in permeable rocks, Geophysics 53 (1988) 519–527.
[27] Y. Bernabe, The frequency dependence of harmonic fluid flow through networks of cracks and pores, Pure Appl. Geophys. 149 (1997) 489–506.
[28] S.R. Pride, M.W. Haartsen, Electroseismic wave properties, J. Acoust. Soc. Am. 100 (1996) 1301–1315.
[29] S.R. Pride, Governing equations for the coupled electromagnetics and acoustics of porous-media, Phys. Rev. B 50 (1994) 15678–15696.
[30] E. Charlaix, A.P. Kushnick, J.P. Stokes, Experimental-study of dynamic permeability in porous-media, Phys. Rev. Lett. 61 (1988) 1595–1598.
[31] M.Y. Zhou, P. Sheng, 1st-principles calculations of dynamic permeability in porous-media, Phys. Rev. B 39 (1989) 12027–12039.
[32] L. Yuan, O.P. Agrawal, A numerical scheme for dynamic systems containing fractional derivatives, J. Vibr. Acoust. 124 (2002) 321–324.
[33] A. Hanyga, Wave propagation in media with singular memory, Math. Comp. Model. 34 (2001) 1399–1421.
[34] I. Podlubny, Fractional Differential Equations, Academic Press, San Diego, 1998.
[35] F.A.L. Dullien, Porous Media: Fluid Transport and Pore Structure, Academic Press, New York, London, 1979.
[36] MA. Biot, General theory of three-dimensional consolidation, J. Appl. Phys. 12 (1941) 155–164.
[37] N.H. Ricker, Transient Waves in Visco-elastic Media, Elsevier, Amsterdam, 1977.
[38] J.F. Lu, J.H. Wang, The scattering of elastic waves by holes of arbitrary shapes in saturated soil, Acta Mech. Sin. 34 (2002) 904–913 (in Chinese).
[39] J. Dvorkin, A. Nur, Dynamic poroelasticity – a unified model with the squirt and the Biot mechanisms, Geophysics 58 (1993) 524–533.
[40] J. Virieux, P-SV wave propagation in heterogeneous medium: velocity–stress finite difference method, Geophysics 51 (1986) 889–901.
[41] R. Gorenflo, F. Mainardi, Fractional calculus: integral and differential equations of fractional order, in: A. Carpinteri, F. Mainardi (Eds.), Fractals and Fractional Calculus in Continuum Mechanics, Springer, Wien and New York, 1997, pp. 223–276.
[42] K. Diethelm, N.J. Ford, A.D. Freed, A predictor–corrector approach for the numerical solution of fractional differential equations, Nonlinear Dyn. 29 (2002) 3–22.
[43] M. Seredyńska, A. Hanyga, Nonlinear Hamiltonian equations with fractional damping, J. Math. Phys. 41 (2000) 2135–2156.
[44] J. Padovan, Computational algorithm for finite element formulation involving fractional operator, Comput. Mech. 2 (1987) 275–282.
[45] M. Enelund, P. Olsson, Damping described by fading memory – analysis and application to fractional derivative models, Int. J. Solids Struct. 36 (1999) 939–970.
[46] P.J. Davis, P. Rabinowitz, Methods of Numerical Integration, Academic Press, Prlando, FL, 1984.
[47] J.M. Carcione, Wave Fields in Real Media: Wave Propagation in Anisotropic, Anelastic, and Porous Media, Pergamon, Amsterdam, 2001.
[48] A.V. Oppenheim, R.W. Schafer, Discrete-time Signal Processing, Prentice-Hall, Englewood Cliffs, NJ, 1999.
[49] R. Kosloff, D. Kosloff, Absorbing boundaries for wave propagation problems, J. Comput. Phys. 63 (1986) 363–376.